Tanzania Journal of Science 45(3): 382-391, 2019 ISSN 0856-1761, e-ISSN 2507-7961

Target-to-Target Interaction in Through-the-Wall Radars under Path Loss Compensated Multipath Exploitation-Based Signal Model for Sparse Image Reconstruction

Emmanuel K Kokumo[1,2], Baraka Maiseli[1], Abdi T Abdalla[1]

[1]*Electronics and Telecommunications Engineering Department, University of Dar es Salaam, Tanzania*

[2]*Electrical Engineering Department, Arusha Technical College, Arusha, Tanzania*

E-mail: ekokumo@ymail.com, barakaezra@udsm.ac.tz, abdit@udsm.ac.tz

Abstract

Multipath caused by reflections from interior walls of buildings has been a long-standing challenge that affects through-the-wall radar imaging. Multipath creates ghost images that introduce confusion when detecting desired targets. Traditionally, multipath exploitation techniques under the compressive sensing framework have widely been applied to address the challenge. However, the multipath component emanating from target-to-target interactions has not been considered–a consequence that may, under multiple target scenarios, lead to incorrect image interpretation. Besides, far targets experience more attenuation due to free space path loss, hence resulting into target undetectability. This study proposes a signal model, based on multipath exploitation techniques, by designing a sensing matrix that incorporates multipath returns due to target-to-target interaction and path loss compensation. The study, in addition, proposes the path loss compensator that, if integrated into the proposed signal model, reduces path loss effects. Simulation results show that the Signal to Clutter Ratio and the Relative Clutter Peak improved by 4.9 dB and 1.9 dB, respectively, compared with the existing model.

Keywords*:* Compressive sensing, multipath ghost, multipath exploitation, path loss, path loss compensator, through-the-wall-radar imaging.

Introduction

Through-the-Wall Radar Imaging (TWRI) refers to an emerging technology that uses Radio Frequency (RF) signals to reveal stationary and moving targets behind opaque obstacles. TWRI finds considerable values in civil and military applications, including rescue missions in fire and earthquake calamities and detection of hidden objects (Yoon and Amin 2010, Tivive et al. 2011, Leigsnering et al. 2014a, Muqaibel et al. 2017, Abdalla et al. 2018). Challenges of TWRI include clutters caused by multipath returns and strong reflections from front walls that pose two additional problems: first, insufficient power transmitted through the wall and reflected back to the radar, leading to missed detections; second, multiple reflections, called ringing or reverberation, within the wall, leading to wall residuals along the range dimension (Setlur et al. 2013, Leigsnering et al. 2014a, 2014b, Abdalla 2016). These problems can, respectively, be addressed by emitting more power, and by refocusing and wall mitigation techniques (Setlur et al. 2011).

Path loss, if insufficiently addressed, may have significant consequences on the scene reconstruction and interpretation. Signals reflected from far targets suffer more path loss attenuation and, therefore, can be unintentionally masked out (Alahmed et al. 2017). This challenge reduces resolution of the reconstructed images representing objects

behind opaque structures. Higher resolutions in radar imaging demand wide bandwidth and large aperture, and these requirements translate to huge data volumes (Tivive et al. 2011, Muqaibel et al. 2014, Leigsnering et al. 2014b, Abdalla et al. 2018). Scholars recommend Compressive Sensing (CS) as a more appropriate approach to address the big data challenge (Yoon and Amin 2008a, Turk et al. 2016). In CS framework, only a small fraction of data is captured to reconstruct images without compromising the image quality (Yoon and Amin 2008a, Turk et al. 2016).

Multipath propagation causes the imaged scene to be populated by unwanted ghost targets, hence reducing sparsity of the scene. Modern research findings revealed that, in terms of image qualities, multipath exploitation-based signal models outperform aspect dependent based counter parts (Abdalla et al. 2018). Recent studies in (Muqaibel and Alkhodary 2012, Leigsnering et al. 2013, Leigsnering et al. 2014b) proposed multipath exploitation based signal models to sparsely reconstruct ghost free images of multiple targets. However, multipath component emanating from target-to-target interaction, which is inevitable under multiple target scenarios, has not been considered, possibly due to its nonlinear behaviour. In addition, the effect of free space loss suggested in Alahmed et al. (2017) has not been addressed under multipath exploitation scenario.

This paper proposes an improved signal model, based on multipath exploitation techniques, which tries to mimic a real TWRI scenario. The contribution of this work lies on the design of the sensing matrix that incorporates multipath returns due to target-to-target interaction and path loss compensation. During image reconstruction, multipath components are exploited to yield ghost-free images and the path loss effect is also compensated using the proposed path loss compensator.

Materials and Methods

TWRI essentials

The TWRI technology employs RF signals to disclose targets located behind the wall. The scene of interest in the wall is mostly interrogated using Stepped-Frequency Radar (SFR) systems. In SFR, a series of M monochromatic waves of linearly increasing frequency are sequentially transmitted at each radar location (Figure 1). The frequency spacing, Δf, is critical because it dictates the maximum unambiguous distance, R_{max}, defined by equation (1) (Yoon and Amin 2008b, Muqaibel and Alkhodary 2012, Wu et al. 2014, Abdalla et al. 2018):

$$R_{max} = \frac{c}{2\Delta f} \qquad (1)$$

where c signifies the speed of the transmitted RF signal.

The downrange resolution, ΔR, expressed in meters, determines the number of transmitted monochromatic waves for a targeted maximum unambiguous range. This quantity, defined by equation (2) (Muqaibel et al. 2017), refers to the ability of the radar system to resolve discrete targets positioned along different downrange locations in the same angular displacement.

$$\Delta R = \frac{c}{2M\Delta f} \qquad (2)$$

The product, $M\Delta f$, defines the signal bandwidth. The mathematical equation (2) explains why modern TWRI systems employ ultra-wideband signals.

The size of the aperture, L, is dictated by the system's cross range resolution, ΔR_C, which refers to the ability of the radar to discriminate adjacent targets resting at the same downrange with different angular displacements. For the Synthetic Aperture Radar (SAR) system of aperture length, L, operating with RF signal of wavelength, λ, imaging two targets located at a range, $\mathcal{R}$, then ΔR_C is given by equation (3) (Abdalla 2018):

$$\Delta R_C = \frac{\lambda \mathcal{R}}{2L} \qquad (3)$$

This is the reason why the modern TWR systems use SAR to realize large aperture once physical array becomes infeasible.

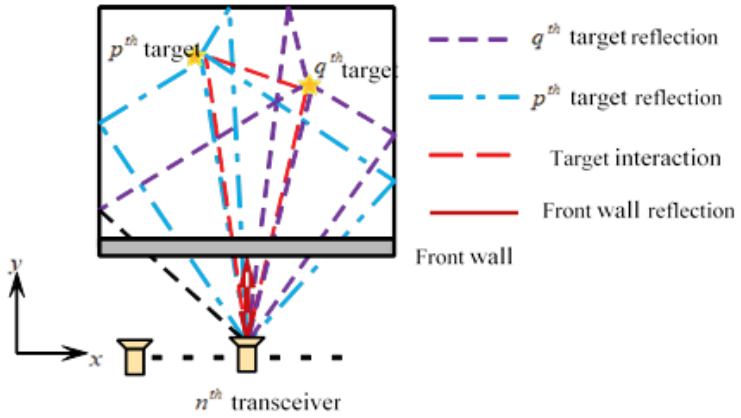

Figure 1: Scene model in through-the-wall radar imaging.

Proposed multipath exploitation-based signal model

To address the challenges of the current multipath exploitation based ghost suppression methods, we propose a CS based multipath ghost suppression method, which suppresses the additional ghost resulting from target-to-target interactions. The developed signal model, also, reverses the unavoidable effect of free space path loss before sparsely reconstructing the images.

Assume *N* wideband transceivers constituting a line array aperture, located parallel to the x-axis, and a step frequency signal consisting of *M* frequencies regularly spaced over a bandwidth $f_{M-1} - f_0$. The overall received signal, $y[m,n]$, corresponding to the m^{th}frequency and the n^{th} transceiver can be expressed as the superposition of the front wall response, $y_w[m,n]$, target returns, $y_t[m,n]$, target interaction, $y_i[m,n]$, and noise sample, $v(m,n)$, as shown by the equation (4)

$$y[m,n] = u(m,n)\big[y_w[m,n] + y_t[m,n] + y_i[m,n]\big] + v(m,n), \quad (4)$$

where $u(m,n)$, the function of distance from the target to the receiver and frequency of the transmitted signal, signifies the path loss compensation. If the scene of interest is subdivided into N_x by N_y pixels along cross range and downrange, respectively, equation (4) can be expressed as equation (5). The variables in this equation represent the following parameters: $u(m,n,p)$, path loss compensation at m^{th} frequency; n^{th}, transceiver for the p^{th}pixel location; $\tau_{pn}^{(r)}$, round-trip propagation delay between the p^{th} target and the n^{th} transceiver; and τ_{pqn}, time delay of the interaction return. Furthermore, σ_p^r denotes the reflectivity of the p^{th} target's pixel, $\sigma_w^{r_w}$ is the reflectivity of the wall pixels due to path r_w, and $\sigma_{pq} = \sigma_p\sigma_q$ is the overall reflectivity when p^{th} and q^{th} targets interact; and, $r = 0,1,\dots,R-1$ and $r_w = 0,1,\dots,R_w - 1$, respectively, are the numbers of multipaths from interior and front walls.

Expressing equation (5) in matrix form, we have equation (6).

$$[m,n] = \sum_{r_w=0}^{R_w-1} u(m,n,p)\left[\sigma_w^{r_w}\exp\left(-j2\pi f_m \tau_w^{r_w}\right) + \sum_{r=0}^{R-1}\sum_{p=0}^{N_xN_y-1}\sigma_p^{(r)}\exp(-j\pi f_m \tau_{pn}^{(r)}) + \sum_{\substack{p,q=0 \\ p\neq q}}^{N_xN_y-1}\sigma_{pq}\exp(-j2\pi f_m \tau_{pqn})\right] + v(m,n), \quad (5)$$

$$\boldsymbol{y} = \sum_{r=0}^{R-1}\mathbf{U}^{(r)}\boldsymbol{\Phi}^{(r)}\,\boldsymbol{s}^{(r)} + \sum_{r_w=0}^{R_w-1}\mathbf{U}_w^{(r_w)}\boldsymbol{\Phi}_{\mathrm{w}}^{(r_w)}\,\boldsymbol{s}_w^{(r_w)} + \mathbf{U}_i^{(0)}\boldsymbol{\Phi}_i^{(0)}\,\boldsymbol{s}_i^{(0)} + \boldsymbol{v}, \quad (6)$$

where $\mathbf{s}^{(\mathrm{r})}$, $\mathbf{s}_{\mathrm{w}}^{(\mathrm{r_w})}$, and $\boldsymbol{s}_i^{(0)} \in \mathrm{C}^{N_xN_y\times 1}$ represent the vectors of reflectivities, σ_p^r, $\sigma_w^{r_w}$, and σ_{pq}^r, respectively. The entries of the matrices $\boldsymbol{\Phi}^{(r)}$, $\boldsymbol{\Phi}_{\mathrm{w}}^{(r_w)}$, and $\boldsymbol{\Phi}_i^{(0)} \in \mathrm{C}^{MN\times N_xN_y}$ are defined as equations (7)–(10)

$$\left[\boldsymbol{\Phi}^{(r)}\right]_{ip} = \exp\left(-j2\pi f_m \tau_{pn}^{(r)}\right), \quad (7)$$

$$\left[\boldsymbol{\Phi}_{\mathrm{w}}^{(r_w)}\right]_{ip} = \exp\left(-j2\pi f_m \tau_w^{(r_w)}\right), \quad (8)$$

$$\left[\boldsymbol{\Phi}_i^{(0)}\right]_{ip} = \exp\left(-j2\pi f_m \tau_{pnq}^{(0)}\right), \text{and} \quad (9)$$

$$\left[\mathbf{U}^{(r)}\right]_{ip} = \left(f_m \tau_{pn}^{(r)}\right)^2, \quad (10)$$

where $m = i \bmod M$ and $n = \left\lfloor \frac{i}{M} \right\rfloor$, $i = 0,1,2,\ldots,MN-1$.

To apply CS theories, the measurement obtained in equation (6) is down-sampled using a binary matrix $\boldsymbol{D} \in \{0,1\}^{J\times MN}$. The matrix $\boldsymbol{D}$ can be thought of as an $MN \times MN$ identity matrix, where all but J rows have been deleted. The under-sampled measurement, $\bar{\boldsymbol{y}}$, is then given by equation (11) (Yoon and Amin 2008a).

$$\bar{\boldsymbol{y}} = \mathbf{D}\boldsymbol{y}. \quad (11)$$

The image of the scene, $\boldsymbol{s}$, defined by equation (6), is reconstructed by solving the optimization problem (12) (Donoho 2006, Yoon and Amin 2008a)

$$\tilde{\boldsymbol{s}} = \arg\min_{\boldsymbol{s}} \|\boldsymbol{s}\|_1 \quad s.t.\ \|\bar{\boldsymbol{y}} - \mathbf{A}\boldsymbol{s}\|_2 < \varepsilon, \quad (12)$$

with

$$\mathbf{A} = \begin{bmatrix} \mathbf{U}^{(0)}\boldsymbol{\Phi}^{(0)} \ldots \mathbf{U}^{(R-1)}\boldsymbol{\Phi}^{(R-1)} & \mathbf{U}_w^{(0)}\boldsymbol{\Phi}_{\mathrm{w}}^{(0)} \ldots \\ \mathbf{U}_w^{(R_w-1)}\boldsymbol{\Phi}_{\mathrm{w}}^{(R_w-1)} & \mathbf{U}_i^{(0)}\boldsymbol{\Phi}_i^{(0)} \end{bmatrix}$$

$$\boldsymbol{s} = \left[\boldsymbol{s}^{(0)} \ldots \boldsymbol{s}^{(R-1)}\ \boldsymbol{s}_w^{(0)} \ldots \boldsymbol{s}_w{}^{(R-1)}\ \boldsymbol{s}_i^{(0)}\right]^T.$$

The choice of ε, which is the function of noise power, is defined in Huang et al. (2010).

Results and Discussions

The TWRI system was implemented using MATLAB software. For fair comparison, the room geometry was taken from Leigsnering et al. (2014b) (Figure 2). The centre of the aperture defined the system's origin, where the right, left, and back walls were positioned at 1.8 *m*, 4 *m*, and 6.37 *m*, respectively. A concrete front wall is located parallel to the array at 2.44 *m* downrange and has a thickness of d = 20 *cm* and relative permittivity of ε = 7.6632. A SAR with 45 predefined locations, linearly spaced by 4.4 *cm*, was used to interrogate the scene sweeping a 2 *m* crossrange distance. At each location, 101 equally spaced frequencies

ranging from 1 *GHz* to 3 *GHz* were transmitted and received using monostatic SFR configuration. Two point targets were located at (0.31, 3.6) *m* and (–0.62, 5.2) *m*. The front wall contribution was mitigated using spatial filtering that was applied before the image reconstruction, as in Lagunas et al. (2013). During simulation, six signal returns were assumed, where the partial path corresponds to the following directions: direct, back-wall multipath, left-side, right-side wall, and target-to-target interaction multipath. In this work, we define a path from the radar to the target or vice versa as partial path.

For simplicity, we assume all side walls to be perfect reflectors. This assumption is justifiable because when the walls are imperfect, the ghost targets will have diminished powers and, therefore, can be easily suppressed. White noise of 0 *dB* Signal-to-Noise Ratio (SNR) was added to the simulated measurements. The Delay and Sum Beam Forming (DSBF) image using full data volume was obtained for benchmarking. For the sparse reconstructions, only half of the radar locations and half of the frequency bins were randomly collected to reconstruct the images using Yall1 algorithm (AlBeladi and Muqaibel 2018).

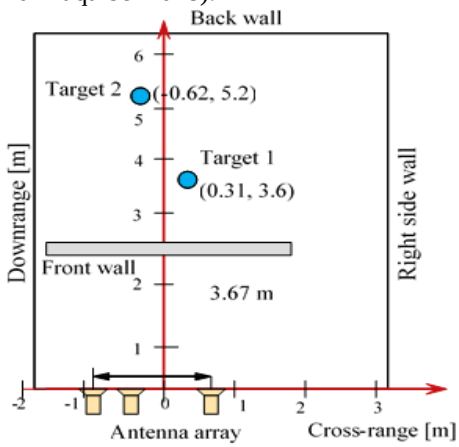

Figure 2: Measurement setup and room layout.

In this section, we present results based on MATLAB simulation with three scenarios implemented. The first scenario assumes two-point targets while the second one assumes three-point targets to observe the effect of target interaction when the number of targets increases. The third scenario simulates the effect of path loss compensation when reconstructing three-point targets.

Scenario 1: Target interactions with two targets

This section analyses the effects of interaction for two-point targets that result to an additional ghost target (Figure 3 (a-c), see cycles). Figure 3 (a) shows an image formed using DSBF with total data volume and Figure 3 (b) is the image formed using conventional CS with only 25% of data volume with SCR and RCP of 26.9 *dB* and 3.5 *dB*, respectively. Figure 3 (c) shows an image reconstructed using the existing multipath exploitation based model whereby the ghost due to target interaction still exist. The corresponding SCR and RCP values are 28.8 *dB* and 10.2 *dB*, respectively. Figure 3 (d) is the image reconstructed with the proposed model in which all ghosts are clearly eliminated and the SCR and RCP are respectively 33.7 *dB* and 12.1 *dB*.

The variations of SCR and RCP with SNR (Figure 4) show that both metrics improve with increasing SNR while the proposed model displays superior performance over the existing one. To investigate the effects of target interaction with increasing number of targets, we increased the number of targets to three.

Scenario 2: Target interactions with three targets

This section analyses the effects of target interaction multipath when increasing the number of targets. An additional target was assumed to be located at (0.71, 1) *m*, and the image qualities using quantitative performances, SCR and RCP, were re-

evaluated. Figure 5 (a) shows a benchmarking image using full data DSBF technique and Figure 5 (b) depicts the conventional CS image using 25% of the available data. Compared with the two-target scenario, the quantitative results registered notable reductions of SCR and RCP to 24 *dB* and to 3.3 *dB*, respectively. Figure 5 (c) shows an image reconstructed using existing multipath exploitation based model, where the number of additional ghosts increased, hence reducing the SCR and RCP values to 24.7 *dB* and to 8.6 *dB*, respectively; but the performance of the proposed model reduced slightly to 28.6 *dB* and to 10.1 *dB* for SCR and RCP values, respectively, as shown in Figure 5 (d). The variations of SCR and RCP with SNR is shown in Figure 6. Both metrics improve with increasing SNR while the proposed model displays superior performance over the existing one.

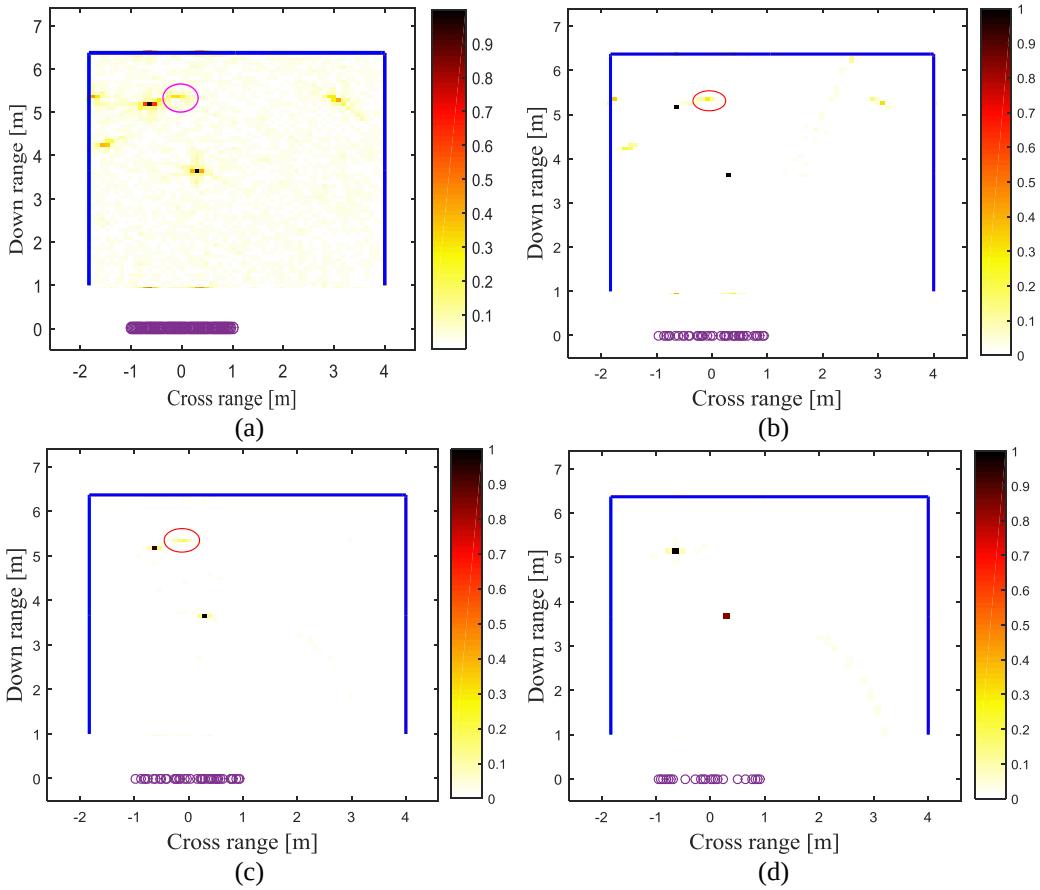

Figure 3: Sparse scene reconstruction (a) DSBF (b) Conventional CS (c) Existing model (d) Proposed model.

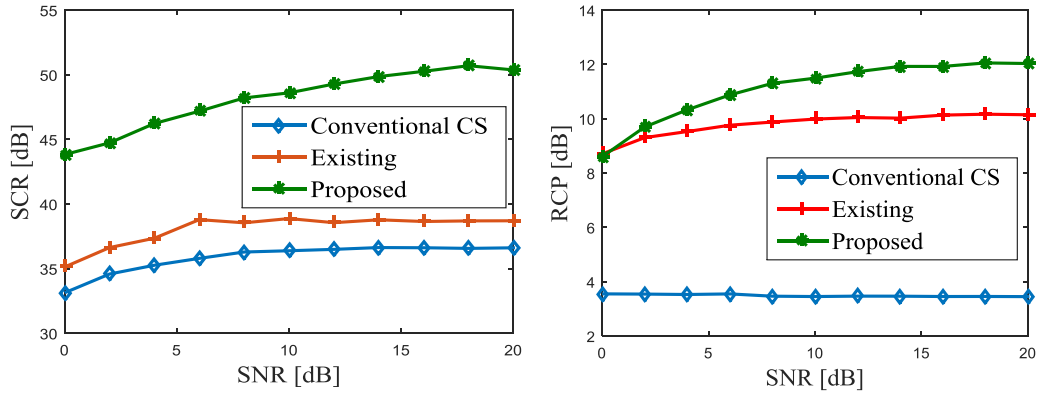

Figure 4: Variation of performance metrics with SNR (a) SCR (b) RCP.

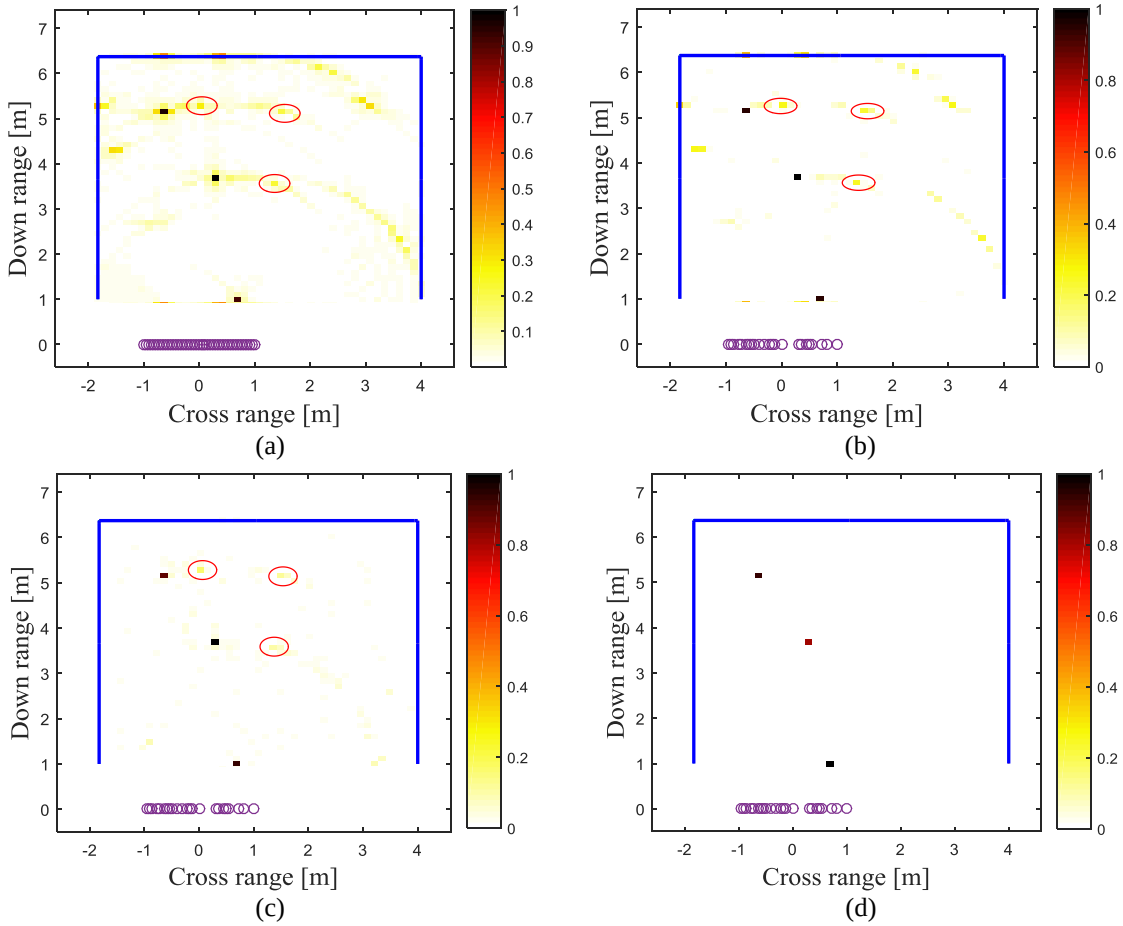

Figure 5: Images of the scene with three point targets (a) DSBF 100% (b) Conventional CS 25% (c) Existing model 25% (d) Proposed model 25%

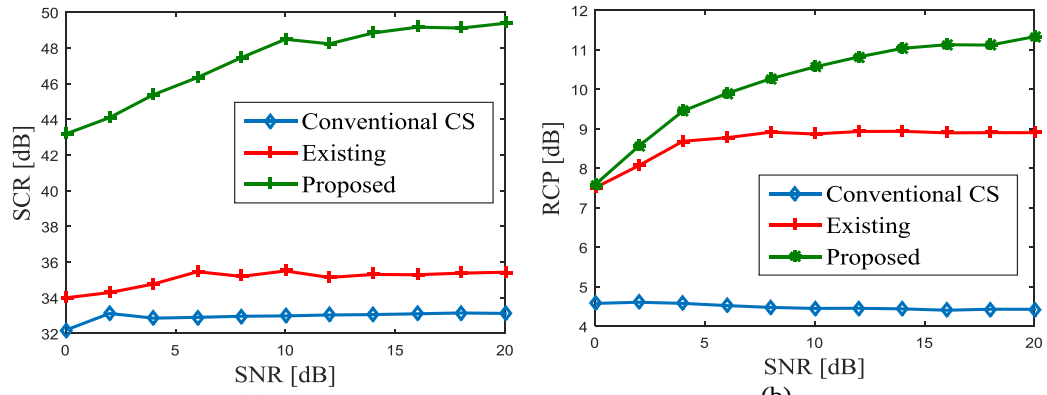

(a) (b)

Figure 6: Variation of performance metrics with SNR (a) SCR (b) RCP.

Scenario 3: Target interactions with path loss compensation

In this section, the performance of the designed path loss compensator is analysed using setup of the preceding scenario, as shown in Figure 7(a). The added nearest target was strategically placed to appreciate the effects of path loss on the far targets because such targets, if uncompensated for the loss of power, suffer a notable effect. Simulation shows that, without compensating for the path loss effect, the furthest target disappeared completely and the near second target appeared with reduced intensity as Figure 7 (b) shows. This observation justifies that the free space path loss, if improperly handled during model design, significantly affects image reconstruction. Applying the proposed path loss compensation technique enabled successful detection of the three targets as shown in Figure 7 (c).

The probability of detection compares the number of detected targets and the number of the available targets, as illustrated in Figure 7 (d). For the threshold below 0.15, the proposed compensator managed to detect 100% of targets compared with only 66% when the path loss was not compensated, which then dropped to 33% detection when threshold exceeds 0.2. This finding demonstrates the effectiveness of the proposed compensator.

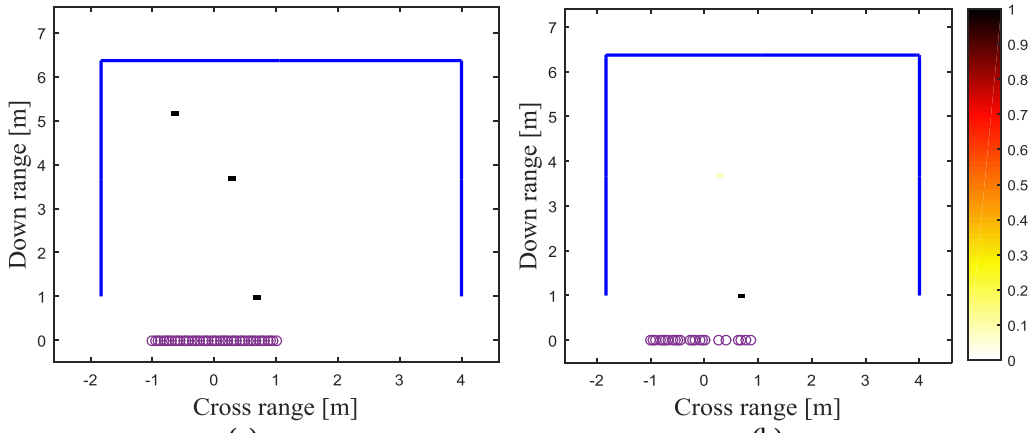

(a) (b)

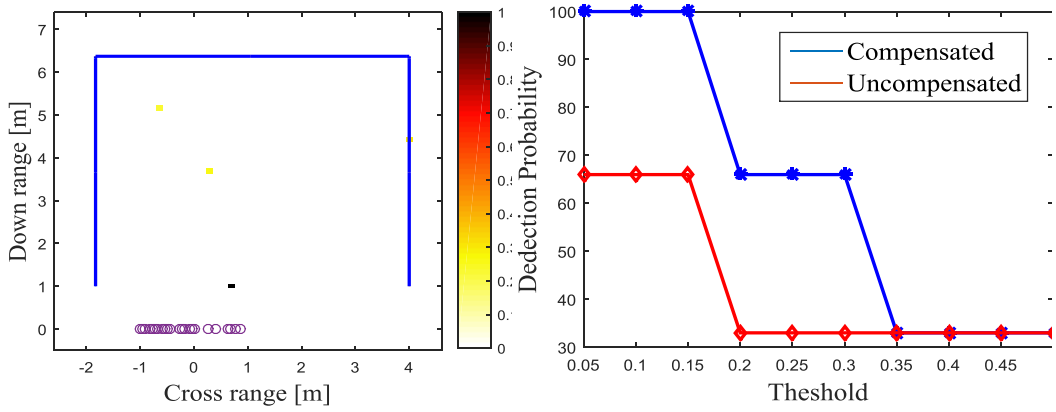

(c) (d)

Figure 7: Reconstructed image (a) Original scene (b) Uncompensated (c) Path loss compensated (d) Detection probability for compensated and uncompensated images.

Conclusions

When dealing with multiple target scenarios in TWRI, target-to-target interaction is inevitable and the associated multipath component should be taken into consideration. Otherwise, the correctness of the scene interpretation will be questionable. Besides, the adverse effect of free-space path loss on different targets may result into masking of some physical targets, if the effect is not properly compensated. This study developed a path loss compensated multipath exploitation based model for multiple target sparse image reconstruction in TWRI. The designed signal model considers both target interaction and path loss compensation, hence making it more realistic and reliable compared with the existing one. Simulation results show significant improvement on SCR and RCP, especially when the number of targets increase, over the existing method. As an extension of this work, further studies may attempt to develop a more effective path loss compensator that exploits extra power associated with all possible multipath returns to enhance quality of the reconstructed targets.

Acknowledgements

This work is funded by the University of Dar es Salaam Competetive Projects, through the directorate of research, award number COICT-ETE 19048.

References

Abdalla AT 2016 *Aspect dependent efficient multipath ghost suppression in TWRI with compressive sensing*. PhD dissertation, King Fahd University of Petroleum and Minerals.

Abdalla AT 2018 Through-the-wall radar imaging with compressive sensing; theory, practice and future trends-A review. *Tanz. J. Sci.* 44(3): 12–30.

Abdalla AT, Alkhodary MT and Muqaibel AH 2018 Multipath ghosts in through-the-wall radar imaging: challenges and solutions. *ETRI Journal* 40(3): 376–388.

Alahmed AS, Alafif OT, Muqaibel AH and Abdalla AT 2017 Path loss compensation in through-the-wall radar imaging. *Proceeding-2016 International Conference on Radar, Antenna, Microwave, Electronics, and Telecommunications (ICRAMET)*, pp. 144–148, Jakarta.

AlBeladi A and Muqaibel AH 2018 Evaluating compressive sensing algorithms in through-the-wall radar via F1-score. *Int. J. Sig. Imag. Sys. Engineering* 11(3): 164–171.

Donoho DL 2006 Compressed sensing. *IEEE*

Transactions on Information Theory 52(4): 1289–1306.

Huang Q, Qu L, Wu B and Fang G 2010 UWB through-wall imaging based on compressive sensing. *IEEE Tran. on Geo. and Rem. Sens*. 48(3): 1408–1415.

Lagunas E, Amin MG, Ahmad F and Nájar M 2013 Wall mitigation techniques for indoor sensing within the compressive sensing framework. *IEEE Trans. Geosci. Remote Sens*. 51(2): 891–906.

Leigsnering M, Amin M, Ahmad F and Zoubir AM 2014a Multipath exploitation and suppression for SAR imaging of building interiors: An overview of recent advances. *IEEE Sig. Proc. Mag*. 31(4): 110–119.

Leigsnering M, Ahmad F, Amin M and Zoubir A 2014b Multipath exploitation in through-the-wall radar imaging using sparse reconstruction. *IEEE Transactions on Aerospace and Electronic Systems* 50(2), 920–939.

Leigsnering M, Ahmad F, Amin M and Zoubir, A 2013 Compressive sensing based specular multipath exploitation for through-the-wall radar imaging. In *IEEE International Conference on Acoustics, Speech and Signal Processing (ICASSP)*, pp. 6004–6008, Vancouver.

Muqaibel AH, Abdalla AT, Alkhodary MT and Al-Dharrab S 2017 Aspect-dependent efficient multipath ghost suppression in TWRI with sparse reconstruction. *Int. J. Microwave Wireless Tech* 9(9): 1839–1852.

Muqaibel AH and Alkhodary MT 2012 Practical application of compressive sensing to ultra-wideband channels. *IET Comm.* 6(16): 2534–2542.

Muqaibel AH, Amin MG and Ahmad F 2014 Directional multipath exploitation for stationary target localization with a single-antenna. In *International Radar Conference: catching the invisible*, Lille.

Setlur P, Alli G and Nuzzo L 2013 Multipath exploitation in through-wall radar imaging via point spread functions. *IEEE Trans. Ima. Proc.: A Publication of the IEEE Signal Processing Society* 22(12): 4571–4586.

Setlur P, Amin M and Ahmad, F 2011 Multipath model and exploitation in through-the-wall and arban radar sensing. *IEEE Trans. Geo. Rem. Sens.* 49(10): 4021–4034.

Tivive F, Amin MG and Bouzerdoum A 2011 Wall clutter mitigation based on eigen-analysisin through-the-wall radar imaging. In *Proc. IEEE Workshop on DSP*, pp. 1–8, Corfu.

Turk A, Ozkan-Bakbak P, Durak-Ata L, Orhan M and Unal M 2016 High-resolution signal processing techniques for through-the-wall imaging radar systems. *Int. J. Microwave Wireless Tech.* 8(6): 855–863.

Wu Q, Zhang YD, Ahmad F, and Amin MG 2014 Compressive-sensing-based high-resolution polarimetric through-the-wall radar imaging exploiting target characteristics. *IEEE Ant. Wireless Prop. Lett*. 14(c): 1043–1047.

Yoon YS and Amin M 2010 Through-The-Wall Radar Imaging Using Compressive Sensing Along Temporal Frequency Domain. In *ICASSP 2010*, pp. 2806–2809, Dallas.

Yoon YS and Amin M 2008a Compressed sensing technique for high-resolution radar imaging. *Proceedings of SPIE Signal Processing, Sensor Fusion and Target Recognition XVII*, pp. 6968(1), Florida.

Yoon YS and Amin M 2008b High resolution through-the-wall radar imaging using extended target model. In *Radar Conference. RADAR '08. IEEE,* pp. 1–4, Rome.